

Transient Performance of a Unified Control System for the Provision of Ancillary Services in Low-Voltage Distribution Networks

Kalliopi D. Pippi, Alexandros D. Boubaris, Georgios C. Kryonidis, Nick P. Papanikolaou
and Theofilos A. Papadopoulos

Abstract—The advent of renewable energy sources (RESs) has posed several technical challenges related to the operation of modern power systems. These can be classified into two main categories: a) problems at the power system level, and b) local problems at the distribution network (DN). To solve these issues, there is a strong need for the development of innovative control schemes that can be employed by converter-based network assets, e.g., battery energy storage (BES) systems and distributed RES. In this context, a unified control system (UCS) for the provision of ancillary services (ASs) by distributed RES-BES systems within a multi-services perspective is introduced in this paper. The proposed UCS comprises different algorithms to provide ASs related to voltage regulation, voltage unbalance mitigation and frequency support. The UCS is implemented in 3-phase, 4-leg converters (3Ph4LCs) to ensure the provision of ASs in unbalanced DNs. In addition, at the dc side of the 3Ph4LC a series dc-dc converter for BES support allows the implementation of the proposed UCS in weak DNs. The transient operational performance of the proposed UCS is evaluated by conducting time-domain simulations.

Keywords—Four-leg converter, frequency support, power oscillation damping, symmetrical components, voltage control, voltage unbalance mitigation.

I. INTRODUCTION

THE ongoing increase of energy prices alongside the environmental concerns on using fossil fuels for energy production necessitate the decarbonisation of the electrical sector [1]. However, the transition from conventional power plants to renewable energy sources (RESs) jeopardizes the reliable operation of the power systems, and especially of distribution networks (DNs). In particular, the volatility of RESs causes new technical challenges related to the grid frequency and the voltage levels of the DNs. For this reason, battery energy storage (BES) systems are situated alongside RESs to provide ancillary services (ASs) to DNs for voltage regulation (VR), voltage unbalance mitigation (VUM) and frequency support (FS) [2].

The research work was supported by the Hellenic Foundation for Research and Innovation (H.F.R.I.) under the "First Call for H.F.R.I. Research Projects to support Faculty members and Researchers and the procurement of high-cost research equipment grant" (Project Number: HFRI-FM17-229).

K. D. Pippi, A. D. Boubaris, N. P. Papanikolaou and T. A. Papadopoulos are with the Power Systems and Power Electronics Laboratories, Department of Electrical and Computer Engineering, Democritus University of Thrace, Xanthi 67100, Greece (e-mail: thpapad@ee.duth.gr).

G. C. Kryonidis is with the School of Electrical and Computer Engineering, Aristotle University of Thessaloniki, Thessaloniki 54124, Greece.

Paper submitted to the International Conference on Power Systems Transients (IPST2023) in Thessaloniki, Greece, June 12-15, 2023.

Focusing on the effective control of network voltages, droop-based approaches constitute the most widely known VR control scheme, since they can be readily integrated to commercial 3-phase converters. In [3]–[5], it has been verified that voltage violations can be effectively tackled by adjusting the active (P) or/and reactive (Q) power at the output of the converter of RES/BES by using droop curves. Nevertheless, in such solutions, either the use of P is prioritized against Q leading to increased BES utilization, or the power losses of the DN are significantly higher due to the increased use of Q . Droop curves can be combined with the damping conductance concept [4] or consensus-based algorithms [5], enabling the phase allocation of P at the output of the converter to ensure the provision of VUM services. However, these solutions lead to conflicting objectives due to the strong coupling between the VR and VUM controls.

In addition, the gradual replacement of rotating generators by converter-based RES contributes to the reduction of the system inertia. To overcome this issue, several solutions have been proposed in the literature dealing with the provision of virtual inertia (VI) from converter-based RES that can be classified into two main categories. In the first category, the concept of the virtual synchronous generator (VSG) is introduced, where the converter of the RES is controlled to imitate the behavior of a synchronous generator [6], [7]. However, additional control loops are needed to address potential converter overloading since the output currents are not actively controlled in the VSG concept, similarly to a synchronous generator. As a result, the synchronization of the VSG with the grid is deteriorated, putting also an extra burden towards the implementation of this solution due to the additional control complexity [8]. In the second category, a phase-locked loop (PLL) is used to measure the network frequency [2], [9]. Based on this measurement, the rate of change of frequency (RoCoF) is calculated and the amount of VI is proportionally determined with respect to the desired inertial constant. It is worth mentioning that this solution is compatible with the majority of the commercially available converters due to the use of the PLL for measuring the network frequency. Such a method is also introduced in [10], where RoCoF is estimated to determine the amount of P that should be absorbed/injected by RES/BES in case of frequency variations. Nevertheless, the use of the PLL may jeopardize the provision of FS, especially in weak grids, due to its slow response and possible oscillations caused during

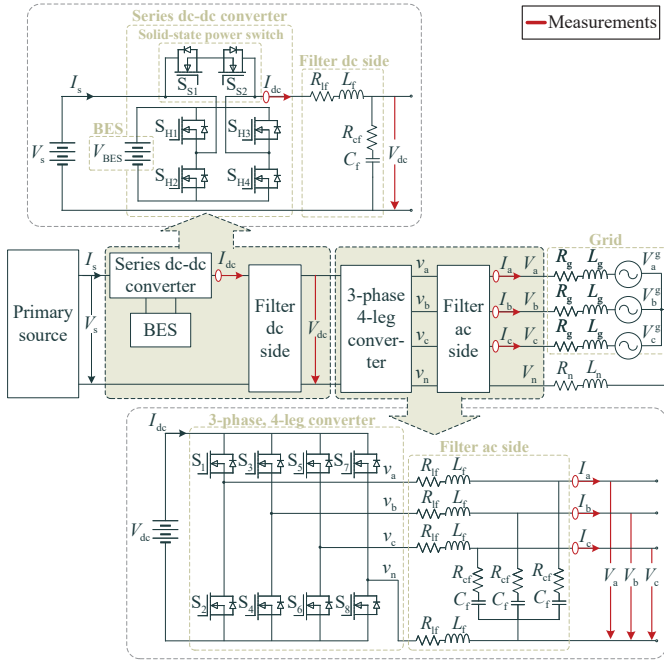


Fig. 1. Model of the proposed UCS.

frequency variations. Therefore, significant research effort has been made to design more advanced PLL schemes, dedicated to grids presenting increased harmonic distortion levels, by mitigating or virtually balancing the point-of-interconnection (POI) parameter variability [11], [12]. However, instead of their optimized performance, they present limited efficacy against the imminent grid transients [13], [14]. For this reason, in [15], cooperative schemes with power stabilization auxiliary services are recommended to optimize the performance of the provided ASs.

In all above studies [3]–[5], [9]–[11], the proposed AS schemes are employed by 3-phase, 3-leg converters, setting limitations regarding their implementation in unbalanced DNs. Thus, new algorithms for the provision of ASs integrated into 3-phase, 4-leg converters (3Ph4LC) are required to expand their applicability [16]. This is merely done in [17], where a feedback-based voltage control scheme is proposed in a 3Ph4LC; however FS is neglected.

In this paper, a unified control system (UCS) implemented in 3Ph4LC is introduced to ensure the provision of multiple ASs by RES/BES in unbalanced DNs. The transient performance of the proposed UCS is investigated and discussed by conducting time-domain simulations. The strengths and contributions of the proposed UCS are:

- *Provision of multiple ASs:* The UCS employs the VR and VUM algorithms presented in [18] to solve voltage problems. Additionally, FS services are provided by the UCS, i.e., VI and primary frequency response (PFR).
- *Introduction of an Auxiliary Control:* An auxiliary power oscillation damping (POD) method is introduced, which uses the series dc-dc converter connected at the dc side of the 3Ph4LC to mitigate PLL oscillations in weak low-voltage (LV) distribution grids, during notable frequency transients.
- *Fully Decoupled Methods:* The proposed control schemes

are implemented in the domain of the symmetrical component removing any coupling interaction.

- *Detailed Converter Modelling:* A 3Ph4LC, a series dc-dc converter and the corresponding operating controls are fully developed in a simulation software.
- *Improved Operation of Conventional Converters:* The proposed UCS can be applied on top of the existing/conventional control schemes that are used in commercial converters, in order to improve their performance without affecting the operating principles.

II. UNIFIED CONTROL SYSTEM MODELLING

The topology of the UCS connected to an unbalanced three-phase DN is depicted in Fig. 1. The DN is modeled as an equivalent Thevenin circuit with three unbalanced voltage sources, i.e., V_a^g , V_b^g and V_c^g , and the corresponding impedances, i.e., $R_g + j\omega L_g$ for each phase and $R_n + j\omega L_n$ for the neutral conductor, where $\omega = 2\pi f$ and f is the grid fundamental frequency.

Compared to conventional 3-phase converters, the 3Ph4LC topology is characterized by three independent legs, i.e., one for each phase, and an additional fourth leg, to ensure the operation in unbalanced DNs [16]. This is achieved by connecting the neutral point of the unbalanced DN in the midpoint of the fourth leg providing a path for the neutral current emerged from the unbalanced operating conditions. The current flow through every converter leg is depended on the state of the switching elements (S₁-S₈) and the phase-to-neutral voltage of the corresponding leg, i.e., v_a , v_b , v_c , or v_n . At the 3Ph4LC output a second-order low-pass filter (LPF) is connected; every phase of the 3Ph4LC filter includes a series resistance, R_{lf} , a series inductance, L_f , a shunt resistance, R_{cf} , and a shunt capacitance, C_f .

Regarding BES integration, compared to the existed solutions where shunt converters are used [19], an H-bridge converter is connected in series to the primary source (a RES unit). Such a topology, allows the direct control of the current at the dc side of the 3Ph4LC reducing the time response of the system, and consequently ensures the reliable operation of the PLL and the efficacy of the 3Ph4LC current controller. The operating principle of the dc-dc converter lies on the necessary BES charging/discharging pattern imposed by the employed VR, FS and POD control schemes. In particular, based on the amount of BES energy needed for ASs provision, a specific voltage value is induced/subtracted by the series H-bridge converter of the BES to properly readjust the dc-link voltage. The high frequency content of the induced/subtracted voltage is filtered by means of a second-order LPF at the dc side of the 3Ph4LC. In addition, a solid-state power switch is connected in parallel with the H-bridge to ensure the uninterrupted operation of the system in case of H-bridge failure.

Dedicated measuring instruments for V_{dc} , I_{dc} , the converter output 3-phase currents I_a , I_b and I_c as well as the phase-to-neutral voltages V_a , V_b and V_c are considered. The obtained measurements are used by the proposed UCS to provide the designed ASs, i.e., VR, VUM and FS, to the DN.

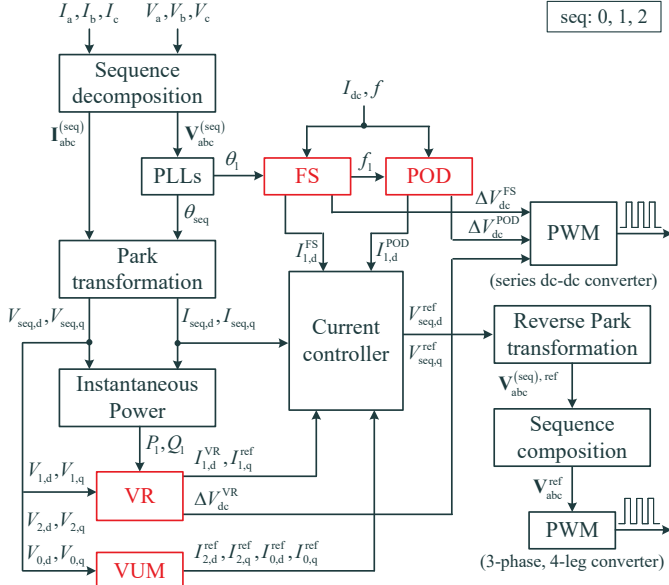


Fig. 2. Block diagram of the proposed UCS.

III. OPERATION OF THE UNIFIED CONTROL SYSTEM

A. Overview

The proposed UCS is depicted by means of block diagram in Fig. 2. The core of the UCS is the transformation of the 3-phase voltage and current measurements at the output of the converter into symmetrical components via (1).

$$\mathbf{X}_{abc}^{(seq)} = \Re(\mathbf{A}_{seq}) \cdot \mathbf{X}_{abc} + \Im(\mathbf{A}_{seq}) \cdot \mathbf{M}_{aux} \cdot \mathbf{X}_{abc} \quad (1)$$

Here, \mathbf{X}_{abc} is either the 3-phase voltage (\mathbf{V}) or current (\mathbf{I}) measurements and subscript $seq = 0, 1, 2$ denotes zero-, positive- and negative-sequence components, respectively. In addition, \mathbf{A}_{seq} is the transformation matrix of each sequence defined as:

$$\mathbf{A}_1 = \frac{1}{3} \begin{bmatrix} 1 & \bar{\alpha} & \bar{\alpha}^2 \\ \bar{\alpha}^2 & 1 & \bar{\alpha} \\ \bar{\alpha} & \bar{\alpha}^2 & 1 \end{bmatrix}, \mathbf{A}_2 = \frac{1}{3} \begin{bmatrix} 1 & \bar{\alpha}^2 & \bar{\alpha} \\ \bar{\alpha} & 1 & \bar{\alpha}^2 \\ \bar{\alpha}^2 & \bar{\alpha} & 1 \end{bmatrix}, \quad (2)$$

$$\mathbf{A}_0 = \frac{1}{3} \begin{bmatrix} 1 & 1 & 1 \\ \bar{\alpha} & \bar{\alpha} & \bar{\alpha} \\ \bar{\alpha}^2 & \bar{\alpha}^2 & \bar{\alpha}^2 \end{bmatrix}$$

where $\bar{\alpha} = 1 \angle \frac{2\pi}{3}$. The auxiliary matrix \mathbf{M}_{aux} given by (3) is used in order to apply a phase shift of $\frac{\pi}{2}$ rad to the measurements [20].

$$\mathbf{M}_{aux} = \begin{bmatrix} 0 & F(s) & F(s) \\ F(s) & 0 & F(s) \\ F(s) & F(s) & 0 \end{bmatrix} \quad (3)$$

Here, $F(s)$ is the transfer function of each second-order LFP in the frequency domain:

$$F(s) = \frac{\omega_g^2}{(s + \omega_g)^2}. \quad (4)$$

The sequence decomposition alongside the fourth leg of the converter enable the independent control of each symmetrical

component. According to this approach, there is no coupling interaction among the zero-, positive- and negative-sequence voltages ($\mathbf{V}_{abc}^{(seq)}$) / currents ($\mathbf{I}_{abc}^{(seq)}$), facilitating their accurate control and ensuring the provision of ASs under unbalanced operating conditions. Specifically, $\mathbf{V}_{abc}^{(seq)}$ is imported into separate PLLs (one PLL for each sequence) to determine the phase signals (θ_{seq}) of each sequence.

Afterwards, using the obtained $\mathbf{V}_{abc}^{(seq)}$, $\mathbf{I}_{abc}^{(seq)}$ and θ_{seq} , the representation of each sequence component at its own rotating reference frame dq0 is acquired according to:

$$\mathbf{X}_{seq,dq0} = \mathbf{T}_{dq0}^{seq} \cdot \mathbf{X}_{abc}^{(seq)} \quad (5)$$

where, \mathbf{T}_{dq0}^{seq} is a matrix describing the Park transformation at each sequence as:

$$\mathbf{T}_{dq0}^{seq} = \frac{2}{3} \begin{bmatrix} \sin(\theta_{seq}) & \sin(\theta_{seq} - \frac{2\pi}{3}) & \sin(\theta_{seq} + \frac{2\pi}{3}) \\ \cos(\theta_{seq}) & \cos(\theta_{seq} - \frac{2\pi}{3}) & \cos(\theta_{seq} + \frac{2\pi}{3}) \\ \frac{1}{2} & \frac{1}{2} & \frac{1}{2} \end{bmatrix}. \quad (6)$$

Considering the estimated $\mathbf{V}_{seq,dq0}$ and $\mathbf{I}_{seq,dq0}$, the instantaneous P and Q of each sequence is calculated as:

$$\begin{bmatrix} P_{seq} \\ Q_{seq} \end{bmatrix} = \frac{3}{2} \begin{bmatrix} V_{seq,d} I_{seq,d} + V_{seq,q} I_{seq,q} \\ V_{seq,q} I_{seq,d} - V_{seq,d} I_{seq,q} \end{bmatrix}. \quad (7)$$

Additionally, the estimated $\mathbf{V}_{seq,dq0}$ is used by the UCS to ensure the provision of VR and VUM. In particular, the positive-sequence voltage of the rotating reference frame dq0 ($\mathbf{V}_{1,dq0}$) as well as the instantaneous positive-sequence active and reactive power (P_1 and Q_1) are used by the VR method. The VUM method receives as inputs the zero- and negative-sequence voltages, $\mathbf{V}_{0,dq0}$ and $\mathbf{V}_{2,dq0}$, respectively. Based on the VR and the VUM control methods, the reference current ($I_{seq,d}^{ref}$ and $I_{seq,q}^{ref}$ where $seq = 0, 1, 2$) for each sequence is determined. Note that, the positive-sequence reference current of d-axis determined by the VR method is equal to $I_{1,d}^{VR}$. The final positive-sequence reference current of d-axis ($I_{1,d}^{ref}$) is estimated according to (8), as the sum of the corresponding reference current determined by the VR method ($I_{1,d}^{VR}$) and the reference currents determined by the FS and POD method ($I_{1,d}^{FS}$ and $I_{1,d}^{POD}$, respectively).

$$I_{1,d}^{ref} = I_{1,d}^{VR} + I_{1,d}^{FS} + I_{1,d}^{POD} \quad (8)$$

Here it should be indicated that since UCS adjusts the current components of the 3Ph4LC by employing dedicated current control loops (CCLs), converter overloading can be avoided by using appropriate saturation blocks. In addition, considering the fact that the capacity of the 3Ph4LC is limited, FS is prioritized against VR and, eventually VUM, in order to avoid violating the technical constraints of the 3Ph4LC.

As reference currents $I_{seq,d}^{ref}$ and $I_{seq,q}^{ref}$ have been determined, the output converter voltages ($V_{seq,d}^{ref}$ and $V_{seq,q}^{ref}$)

of each sequence at the rotating reference frame dq0 are estimated as:

$$\begin{bmatrix} V_{\text{seq},d}^{\text{ref}} \\ V_{\text{seq},q}^{\text{ref}} \end{bmatrix} = \begin{bmatrix} I_{\text{seq},d}^{\text{ref}} - I_{\text{seq},d} \\ I_{\text{seq},q}^{\text{ref}} - I_{\text{seq},q} \end{bmatrix} \left(k_{p,\text{sec}} + \frac{k_{i,\text{sec}}}{s} \right) + \begin{bmatrix} -I_{\text{seq},q} \\ I_{\text{seq},d} \end{bmatrix} \omega_g L_f + \begin{bmatrix} V_{\text{seq},d} \\ V_{\text{seq},q} \end{bmatrix} \quad (9)$$

where $k_{p,\text{seq}}$ and $k_{i,\text{seq}}$ are the proportional and the integral gains of six different proportional-integral (PI) controllers (two identical PIs for each sequence), respectively. The voltage reference per phase of each symmetrical component ($\mathbf{V}_{\text{abc}}^{(\text{seq}),\text{ref}}$) are calculated by using the reverse Park transformation.

By adding the corresponding symmetrical voltages $\mathbf{V}_{\text{abc}}^{(\text{seq}),\text{ref}}$, the 3-phase voltages ($\mathbf{V}_{\text{abc}}^{(\text{ref})}$) are estimated. Eventually, utilizing the $\mathbf{V}_{\text{abc}}^{(\text{ref})}$ and conventional PWM methods, the proper pulse sequence of the switching elements of the 3Ph4LC is determined.

B. Provision of VR and VUM Services

The VR control scheme presented in [18] is adopted by the proposed UCS. According to this method, VR is achieved by the coordinated operation of a central and a local controller (CC and LC, respectively). The operation schemes of the CC and the LC are depicted in the flowcharts of Figs. 3(a) and 3(b), respectively. The CC is used to send the necessary control signals to the LC in case a voltage violation incident is detected. The latter one is integrated into the 3Ph4LC and sends data, i.e., the positive-sequence voltage V_1 of POI and an auxiliary binary variable b_{aux} , to the CC. Additionally, the LC adjusts the 3Ph4LC output power based on the signals received from the CC following the rule-based strategy described below.

The VR algorithm incorporated in the LC of the 3Ph4LC consists of two operating modes, namely M1 and M2. To avoid oscillations and switching actions between these modes, they are separated by a small dead-band (db), where the VR algorithm remains deactivated.

In particular, M1 is employed to regulate the positive-sequence voltage V_1 into predefined limits giving priority to the utilization of Q_1 against P_1 . Note that, V_1 is calculated as the average value of $V_{1,d}$ by means of a moving average window filter. This operating mode is activated by a proper signal (AS_{M1}) sent by the CC to the LC, when V_1 violates the permissible voltage limits ($V_{\text{lim}}^{\text{min}}$, $V_{\text{lim}}^{\text{max}}$). In case a voltage violation occurs ($AS_{M1} = 1$), b_{aux} is set equal to 1 and is also transmitted from the LC to CC, to denote that the VR algorithm has been enabled. Since M1 is activated to the LC, the available amount of Q_1 of the 3Ph4LC is initially used as the only means of VR. The reference positive-sequence reactive power (Q_1^{ref}) that should be absorbed/injected by the 3Ph4LC is determined by (10):

$$Q_1^{\text{ref}} = (V_{\text{ref}} - V_1) \left(k_p^{\text{VR}} + \frac{k_i^{\text{VR}}}{s} \right) \quad (10)$$

where k_p^{VR} and k_i^{VR} are the proportional and the integral gains of a PI controller, respectively. Furthermore, V_{ref} stands for the reference voltage level and is equal to $V_{\text{lim}}^{\text{max}} - 0.5db$,

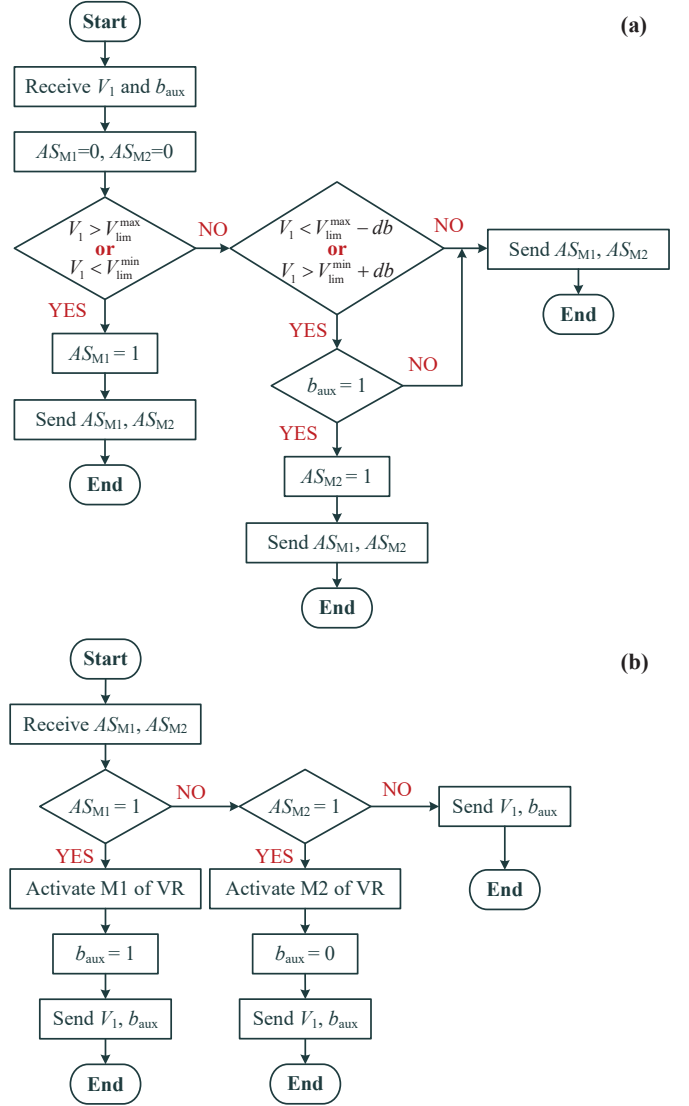


Fig. 3. Flowchart of the operation of (a) the CC and (b) the LC.

in case of an over-voltage incident, or $V_{\text{lim}}^{\text{min}} + 0.5db$ for under-voltage events. This process is repeated till either the voltage is regulated, or the maximum available reactive power (Q_{max}) is reached. Q_{max} is estimated as:

$$Q_{\text{max}} = \sqrt{S_1^2 - P_1^2} \quad (11)$$

Here, S_1 is the nominal apparent power of the converter and P_1 is the active power absorbed/injected by the converter during the control.

If Q_1^{ref} reaches Q_{max} or the voltage violation event is not effectively tackled, P_1 of the 3Ph4LC also participates in the VR process. Specifically, P_1^{ref} , that should be absorbed/injected by the 3Ph4LC is estimated by employing a PI controller similar to (10). Additionally, during the calculation of P_1^{ref} , Q_1^{ref} is constantly readjusted to a new value according to (11), to ensure that the 3Ph4LC absorbs/injects Q_{max} without violating its technical constraints. Afterwards, the voltage difference ($\Delta V_{\text{dc}}^{\text{VR}}$) that should be applied at the dc bus from the series dc-dc converter (see Fig. 1) is calculated by dividing P_1^{ref} and I_{dc} , to achieve

the charging/discharging process of the BES. Utilizing a proportional term, ΔV_{dc}^{VR} is interpreted to the required duty cycle of the series dc-dc converter. This process is repeated till either the voltage is regulated, or the maximum available active power (P_{max}), estimated by (12), is reached.

$$P_{max} = \frac{S_1}{pf} \quad (12)$$

Here, pf stands for the nominal power factor of the 3Ph4LC.

After M1 is completed, the VR control scheme remains idle. However, different network operating conditions may lead to unnecessary power absorption/injection by the 3Ph4LC. For this reason, the CC transmits a proper signal (AS_{M2}) to activate M2, if $b_{aux} = 1$ and either when V_1 decreases below $V_{lim}^{max} - db$ (in case where over-voltage events were previously detected), or when V_1 is higher than $V_{lim}^{min} + db$ (in case where under-voltages were previously observed). During M2, priority is given to the P_1 control of the 3Ph4LC to avoid possible unnecessary use of BES. Thus, when $AS_{M2} = 1$, P_1 of the 3Ph4LC is initially adjusted, until voltage V_1 is regulated or P_1 is zero. In the latter case, Q_1 is reduced till zero ($b_{aux} = 0$), unless the voltage is regulated. Finally, in both M1 and M2, the reference positive-sequence current of q-axis ($I_{1,q}^{ref}$) and $I_{1,d}^{VR}$ are calculated according to (13) and (14), respectively.

$$I_{1,q}^{ref} = -\frac{2}{3} \frac{Q_1^{ref}}{V_{1,d}} \quad (13)$$

$$I_{1,d}^{VR} = \frac{2}{3} \frac{P_1^{ref}}{V_{1,d}} \quad (14)$$

Regarding the adopted VUM method, it has been considered that voltage unbalances are mitigated by controlling the zero- and negative-sequence Q at the output of the 3Ph4LC. This is achieved by the effective regulation of I_0 and I_2 . Specifically, the reference current of each sequence at q-axis, i.e., $I_{0,q}^{ref}$ and $I_{2,q}^{ref}$, that should be absorbed from/injected by the converter, is determined according to (15) and (16), respectively.

$$I_{0,q}^{ref} = B_0 V_{0,d} \quad (15)$$

$$I_{2,q}^{ref} = B_2 V_{2,d} \quad (16)$$

Here, B_0 and B_2 denote the zero- and negative-sequence damping susceptance, respectively. Furthermore, according to the selected VUM algorithm, the corresponding reference currents of d-axis ($I_{0,d}^{ref}$ and $I_{2,d}^{ref}$) are considered zero.

C. Provision of FS and Auxiliary POD Control

Focusing on the employed algorithms related to the FS, i.e., VI and PFR, the positive-sequence phase signal (θ_1), f and I_{dc} are used as inputs.

Regarding VI provision, frequency (f_1) is calculated as the derivative of θ_1 and RoCoF is determined as:

$$RoCoF = \frac{f_1 - f_1^{\Delta t_x}}{\Delta t_x} \quad (17)$$

where $f_1^{\Delta t_x}$ is the delayed value of f_1 . The estimated RoCoF is multiplied by $2H$ to calculate the required amount of injected/absorbed active power (P_1^{VI}) for VI. Note that, H denotes the inertia constant. The final value of active power

(P_1^{FS}) is determined by adding an extra amount of active power (P_1^{PFR}), estimated according to (18), in the P_1^{VI} , to emulate PFR.

$$P_1^{PFR} = D(f_1 - f_n) \quad (18)$$

Here, D stands for the slope of the PFR droop curve [21] and f_n is the grid nominal frequency. Then, the inertia current ($I_{1,d}^{FS}$) (See Eq. (8)) is calculated by dividing the P_1^{FS} with the $V_{1,d}$. Similar to the VR process, by dividing P_1^{FS} with I_{dc} , the corresponding voltage difference, i.e., ΔV_{dc}^{FS} , is estimated and consequently the required duty cycle of the series dc-dc converter is determined.

To deal with the inherited vulnerability of classical PLLs against abrupt RoCoF events and ensure the reliable operation of the UCS in weak grids, the POD control scheme is introduced alongside the FS. In particular, the POD algorithm operates by observing I_{dc} trajectory to focus on more reliable physical magnitudes. This way, the proposed scheme mitigates the impact of the PLL error during transients by partially untangling its response. Eventually, active power balancing and VI support are provided in cooperation with the basic CCLs.

In the same sense, the rate of change of current (RoCoI) is calculated by comparing I_{dc} to its delayed value $I_{dc}^{\Delta t_x}$ according to (19).

$$RoCoI = \frac{I_{dc} - I_{dc}^{\Delta t_x}}{\Delta t_x} \quad (19)$$

RoCoI is introduced into a PI controller with gains k_p^{POD} and k_i^{POD} and the obtained value is multiplied by a compensation term (K) to determine the reference value of $I_{1,d}^{POD}$ (See Eq. (8)) as follows:

$$I_{1,d}^{POD} = K RoCoI \left(k_p^{POD} + \frac{k_i^{POD}}{s} \right). \quad (20)$$

Similar to VR and FS, the required voltage difference related to the POD control (ΔV_{dc}^{POD}) is estimated as:

$$\Delta V_{dc}^{POD} = \frac{G}{K} I_{1,d}^{POD} \quad (21)$$

where, G is a compensation term. Finally, ΔV_{dc}^{POD} is interpreted to the required duty cycle of the series dc-dc converter.

IV. SIMULATION RESULTS

To validate the transient performance of the proposed UCS, time-domain simulations have been conducted in MATLAB Simulink [22]. Two scenarios are examined. In the first scenario, the provision of ASs referring to voltage control is investigated and in the second, the operation of the proposed FS and the POD methods. Note that each AS is examined separately for demonstration purposes and not in terms of the adopted prioritization procedure. The obtained results are presented and discussed in detail in the following subsections.

TABLE I
PARAMETERS OF VOLTAGE CONTROL SIMULATIONS

Parameter	Value	Parameter	Value
R_g	2.7266 Ω	L_g	2.893 mH
R_n	0.9089 Ω	L_n	0.964 mH
R_{lf}	0.0010 Ω	L_f	0.790 mH
R_{cf}	0.1500 Ω	C_f	2.000 μF
$k_{p,0}$	27.0087 V/A	$k_{i,0}$	189 V/A
$k_{p,1}$	12.2767 V/A	$k_{i,1}$	270 V/A
$k_{p,2}$	27.0087 V/A	$k_{i,2}$	405 V/A
k_p^{VR}	0.04 A	k_i^{VR}	0.44 A
V_2^{mag}	1 %	V_0^{mag}	1 %
V_1^{mag}	277.13 V	V_{base}	230.94 V
db	0.23 V		

A. Voltage Control Simulations

The provision of VR and VUM services by the is examined for demonstration purposes assuming an 1 kVA 3Ph4LC and the parameters of Table I; to focus on transient performance of the 3Ph4LC, the operation of the CC is not taken into account in this analysis. Note that, V_2^{mag} and V_0^{mag} stand for the ratio of the negative- and zero-sequence network voltage magnitudes to the corresponding positive-sequence voltage magnitude (V_1^{mag}), respectively; V_{base} denotes the nominal rated network voltage. In this scenario the over-voltage and unbalance problems initiate at $t_0 = 0$ s considering that both active and reactive power output of the 3Ph4LC is zero. Over-voltage incidents are identified, if V_1 at the POI of the 3Ph4LC is higher than $V_{\text{lim}}^{\text{max}} = 1.1$ p.u. [13].

Simulation results are depicted in Figs. 4 – 6. In Fig. 4 the responses of the symmetrical current components of the 3Ph4LC at the rotating reference system dq0 are presented. The profiles of the zero- (V_0), negative- (V_2) and positive-sequence (V_1) voltage components at the output of the 3Ph4LC are depicted in Fig. 5. Finally, Fig. 6 shows the P and Q responses that are absorbed/injected by the 3Ph4LC in symmetrical components; positive P and Q values denote power absorption.

Regarding VUM, an increase of $I_{0,q}$ and $I_{2,q}$ at time instant $t_1 = 1$ s denoting the activation of the VUM method is shown in Figs. 4(a) and 4(b), respectively. In particular, from Fig. 5(a), it is verified that the increase of $I_{0,q}$ leads to decreased V_0 values, i.e., from 2 V to 1.43 V, and consequently to reduced voltage unbalance. Similar remarks are also drawn for V_2 that is reduced from 2.15 V to 1.47 V (See Fig. 5(b)), due to VUM activation. From Figs. 6(a) and 6(b), it can be realized that the reactive power (Q_0 and Q_2) acts as the only means for VUM as both P_0 and P_2 remain zero.

Considering over-voltage, the operation of both M1 and M2 modes of the VR method is evaluated. In Fig. 4(c), $I_{1,q}$ starts increasing at $t_2 = 2$ s according to (13), as V_1 exceeds 254.03 V, i.e., $V_{\text{lim}}^{\text{max}} = 1.1$ p.u., (see Fig. 5(c)). As $I_{1,q}$ increases, Q_1 of the 3Ph4LC increases accordingly (see Fig. 6(c)), and acquires its maximum value, i.e., $Q_{\text{max}} = 1$ kVar, at $t_3 = 3.04$ s. It should be noted that $I_{1,d}$ remains

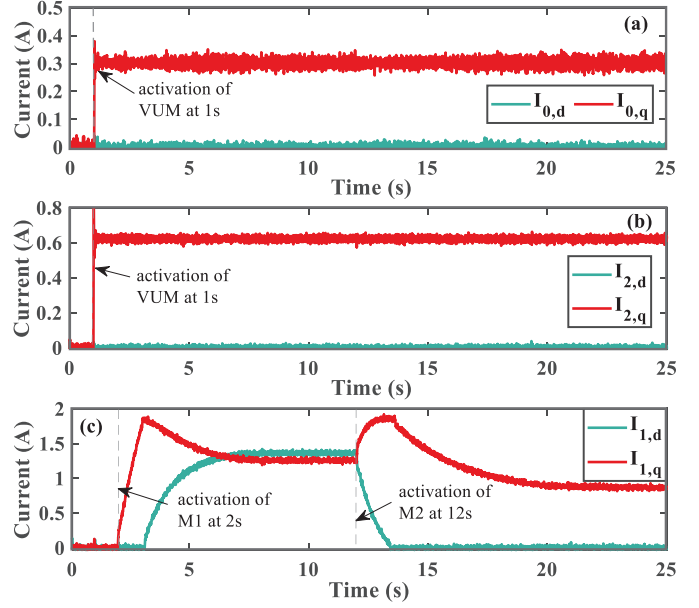


Fig. 4. Current output response of the 3Ph4LC in the dq0 frame for the (a) zero-, (b) negative- and (c) positive-sequence component.

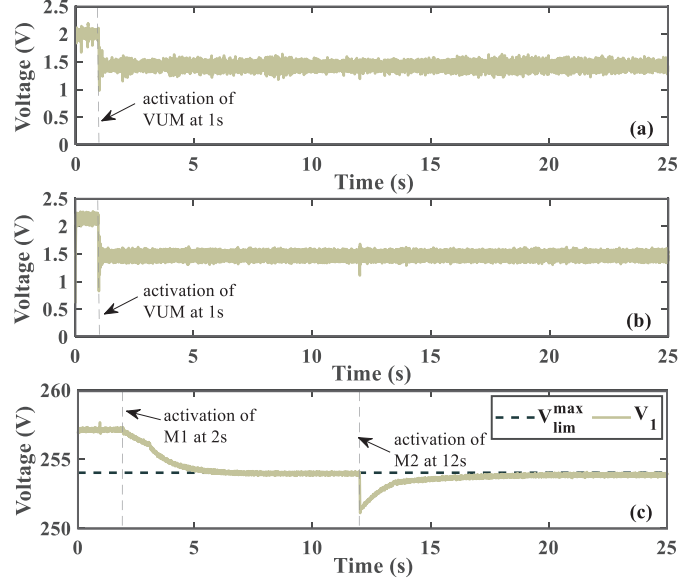


Fig. 5. Voltage response of the (a) zero- (b) negative- and (c) positive-sequence component.

zero until t_3 , since the VR method prioritizes the use of the available Q_1 . From Fig. 5(c), it can be observed that the absorption of Q_{max} does not efficiently tackle the voltage violation incident as $V_1 = 255.98$ V. Therefore, at t_3 the BES charging process is activated, in order to regulate V_1 via P_1 absorption. As a result, $I_{1,d}$ increases leading to a corresponding increase of P_1 as shown in Figs. 4(c) and 6(c), respectively. From Fig. 6(c) it is verified that as P_1 increases, the amount of the absorbed Q_1 is constantly readjusted according to (11), on the basis of the technical constraints of the 3Ph4LC. From Fig. 5(c) it can be realized that V_1 is regulated at $t_4 = 7.1$ s and in order to maintain V_1 within the permissible limits the 3Ph4LC continues to absorb Q_1 and P_1 .

At $t_5 = 12$ s, an intentional grid event occurs and the grid voltage level is reduced ($V_1^{\text{mag}} = 274.13$ V), leading

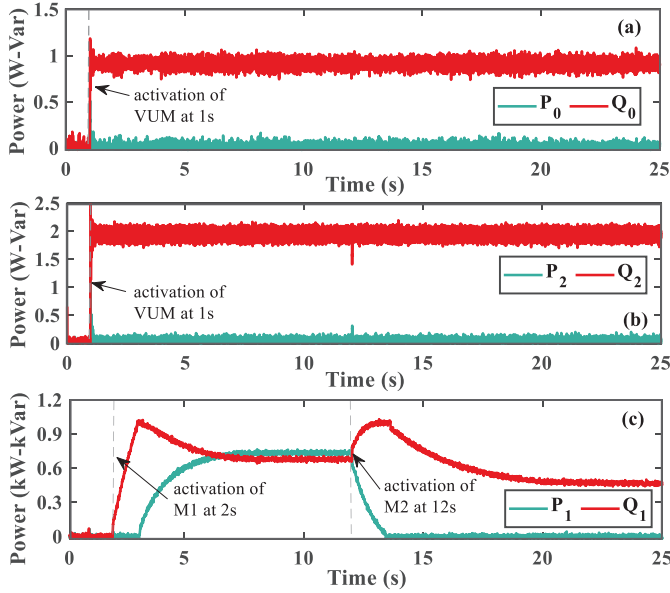


Fig. 6. Active and reactive power output response of the (a) zero-, (b) negative- and (c) positive-sequence component.

TABLE II
PARAMETERS OF FREQUENCY CONTROL SIMULATIONS

Parameter	Value	Parameter	Value
R_g	0.468 Ω	R_N	0.156 Ω
k_p^{POD}	0.04	k_i^{POD}	0.44
t_x^{POD}	0.02 s	t_x^{VI}	0.5 s
D	4 W/Hz	G	57 Vs/A
H	2 s	K	72 s

to a decrease of V_1 below $V_{\text{lim}}^{\text{max}} - db$. This results in the activation of M2. As shown in Figs. 4(c) and 6(c), the decrease of current $I_{1,d}$ and consequently P_1 of BES lead to the increase of V_1 (See Fig. 5(c)). Since $I_{1,d}$ is zero and V_1 is not efficiently regulated, the VR algorithm moves to the reduction of $I_{1,q}$ and to the decrease of Q_1 . Eventually, as V_1 has been regulated at $t_6 = 22.52$ s, the VR control process is deactivated and the 3Ph4LC absorbs only the required amount of Q_1 to maintain V_1 within permissible limits. Thus, the unnecessary BES utilization and reactive power absorption that may lead to increased network power losses are avoided [18].

It is important to indicate that from Figs. 4 – 6 it is evident that the VR and VUM controls are fully decoupled.

B. Frequency Support Simulations

In the second scenario, the FS AS is examined. In general, the parameters of Table I are also considered in this scenario. However, to assess the performance of the FS and POD methods in weak LV distribution grids, a 5 kVA 3Ph4LC is employed and specific simulation parameters are modified as presented in Table II. Note that, during the simulation the provision of PFR service is assumed deactivated, in order to stress out the effect of VI.

Initially, at $t_1 = 0.8$ s, f_1 increases from 50 Hz to 50.5 Hz with a rate of +1 Hz/s up to $t_2 = 1.3$ s as shown in Fig. 7(a). Note that, this value has been selected as RoCoF

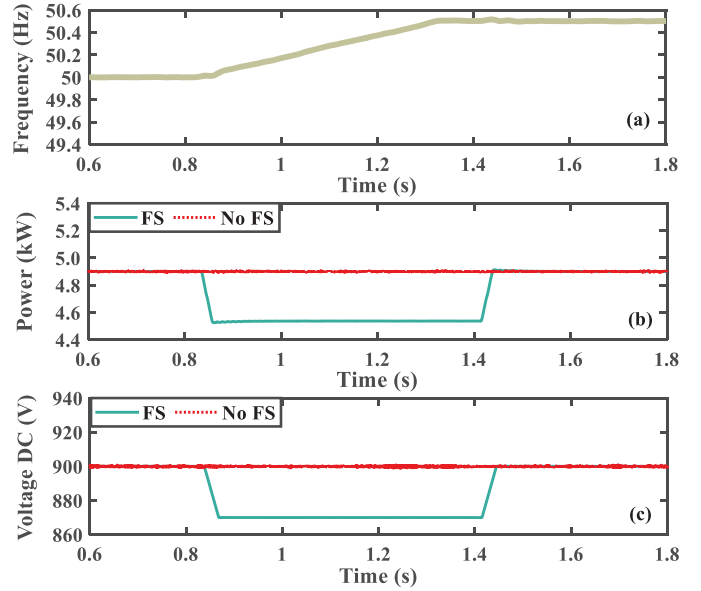


Fig. 7. (a) High-frequency disturbance, (b) output power of the 3Ph4LC and (c) voltage at the dc bus.

up to 1 Hz/s is considered currently manageable with respect to existing power plant units [14]. This way and considering the selected H value, the provision of VI services to the grid is verified, since the P_1 of the 3Ph4LC decreases by 400 W, i.e., $2H \cdot \text{RoCoF} / f = -0.08$ p.u. (See Fig. 7(b)). Moreover, from Fig. 7(c) it can be seen that in the same time period, V_{dc} decreases due to the BES charging process enabled by the series dc-dc converter. In the case of frequency decrease, similar remarks can be deduced.

Additionally, to investigate the efficiency of the POD method, simulations are conducted considering a significant high RoCoF of -6 Hz/s. This is imperative based on the new interpolability standards, e.g., IEEE 2030, that set wider ride-through requirements for RESs, ensuring so the uninterrupted system support, even under high disturbances [13], [14]. Note that, during the conducted simulations the provision of VI is deactivated. The grid RoCoF starts varying at t_1 , till f_1 becomes 47 Hz at t_2 (see Fig. 8(a)). In Figs. 8(b)-(d) results considering POD control ON and OFF are presented. From these figures it is evident that the power disturbances at the output of the 3Ph4LC are mitigated due to the activation of the POD control, when a disturbance of I_{dc} at the dc bus is detected. Finally, according to 8(d), it can be realized that V_{dc} is properly adjusted according to the employed POD algorithm.

V. CONCLUSIONS

The proposed operation scheme is based on a UCS which can support multi-ASs via a combination of converter topologies to solve local issues. The implementation of the UCS in 3Ph4LCs is presented in detail and its efficiency is verified via simulations.

The proposed UCS can regulate the voltage levels prioritizing the reactive power against the active power, leading to reduced BES utilization and consequently to increased BES lifetime expectancy. Moreover, the UCS achieves to mitigate

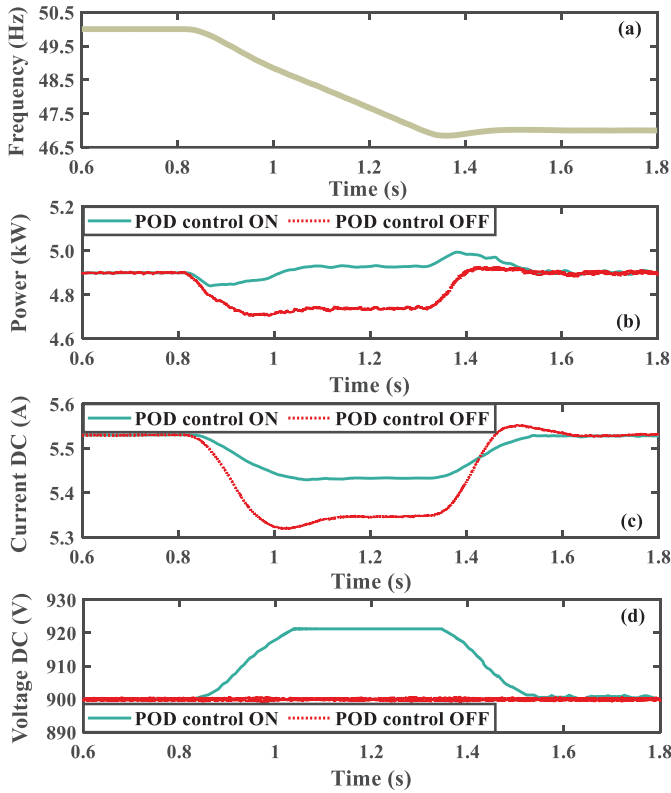


Fig. 8. (a) Frequency and (b) output power of the 3Ph4LC, (c) current and (d) voltage at the dc bus.

the voltage unbalances even in cases where the negative- and zero-sequence voltage levels are below 1 %.

Finally, by employing a series dc-dc converter and appropriate algorithms, the UCS can provide ASs related to the control of the frequency, i.e., provision of VI, PFR, and smoothing of power disturbances at the output of the 3Ph4LC.

As future work, the UCS scheme will be also extended to apply to grid-forming converters. Furthermore, detailed RES and BES models will be employed to assess the provision of ASs.

REFERENCES

- [1] M. Jafari, A. Botterud and A. Sakti, "Decarbonizing power systems: A critical review of the role of energy storage," *Renew. Sustain. Energy Rev.*, vol. 158, p. 112077, 2022.
- [2] G. Kryonidis, E. Kontis, T. Papadopoulos, K. Pippi, A. Nousedilis, G. Barzegkar-Ntovom, A. Boubaris and N. Papanikolaou, "Ancillary services in active distribution networks: A review of technological trends from operational and online analysis perspective," *Renew. Sustain. Energy Rev.*, vol. 147, p. 111198, 2021.
- [3] T. Mai, A. N. Haque, P. Vergara, P. Nguyen and G. Pemen, "Adaptive coordination of sequential droop control for PV inverters to mitigate voltage rise in PV-rich LV distribution networks," *Electr. Power Syst. Res.*, vol. 192, p. 106931, 2021.
- [4] D. Bozalakov, J. Laveyne, J. Desmet and L. Vandeveldel, "Overvoltage and voltage unbalance mitigation in areas with high penetration of renewable energy resources by using the modified three-phase damping control strategy," *Electr. Power Syst. Res.*, vol. 168, pp. 283–294, 2019.
- [5] C. Burgos-Mellado, J. Llanos, E. Espina, D. Saez, R. Cardenas, M. Sumner and A. Watson, "Single-phase consensus-based control for regulating voltage and sharing unbalanced currents in 3-wire isolated AC microgrids," *IEEE Access*, vol. 8, pp. 164 882–98, 2020.
- [6] U. Markovic, Z. Chu, P. Aristidou and G. Hug, "Lqr-based adaptive virtual synchronous machine for power systems with high inverter penetration," *IEEE Trans. Sustain. Energy*, vol. 10, no. 3, pp. 1501–1512, 2019.

- [7] L. Huang, H. Xin, H. Yuan, G. Wang, and P. Ju, "Damping effect of virtual synchronous machines provided by a dynamical virtual impedance," *IEEE Trans. Energy Conv.*, vol. 36, no. 1, pp. 570–573, 2021.
- [8] Z. Qu, J. C.-H. Peng, H. Yang, and D. Srinivasan, "Modeling and analysis of inner controls effects on damping and synchronizing torque components in VSG-controlled converter," *IEEE Trans. Energy Conv.*, vol. 36, no. 1, pp. 488–499, 2021.
- [9] V. Mallemaci, F. Mandrile, S. Rubino, A. Mazza, E. Carpaneto and R. Bojoi, "A comprehensive comparison of virtual synchronous generators with focus on virtual inertia and frequency regulation," *Electr. Power Syst. Res.*, vol. 201, p. 107516, 2021.
- [10] J. Fang, R. Zhang, H. Li and Y. Tang, "Frequency derivative-based inertia enhancement by grid-connected power converters with a frequency-locked-loop," *IEEE Trans. Smart Grid*, vol. 10, no. 5, pp. 4918–27, 2019.
- [11] T. Qoria, E. Rokrok, A. Bruyere, B. Francois and X. Guillaud, "A PLL-free grid-forming control with decoupled functionalities for high-power transmission system applications," *IEEE Access*, vol. 8, pp. 197 363–78, 2020.
- [12] Y. Khayat, S. Golestan, J. Guerrero, J. Vasquez and H. Bevrani, "DC-link voltage control aided for the inertial support during severe faults in weak grids," *IEEE J Emerging and Selected Topics Power Electron.*, vol. 9, no. 6, pp. 7296–7305, 2021.
- [13] *IEEE Standard for Interconnection and Interoperability of Distributed Energy Resources with Associated Electric Power Systems Interfaces*, IEEE Std 1547-2018 (Revision of IEEE Std 1547-2003), 2018, pp. 1–138.
- [14] "CIGRE JWG C2/C4. Impact of high penetration of inverter-based generation on system inertia of networks," *CIGRE TB 851*, 2021.
- [15] *ENTSO-E: Continental Europe Synchronous Area Separation on 08 January 2021*, ICS Investigation Expert Panel, 2021.
- [16] F. Rojas, R. Cárdenas, C. Burgos-Mellado, E. Espina, J. Pereda, C. Pineda, D. Arancibia and M. Diaz, "An overview of four-leg converters: Topologies, modulations, control and applications," *IEEE Access*, vol. 10, pp. 61 277–325, 2022.
- [17] J. Olives-Camps, J. Mauricio, M. Barragan-Villarejo and F. Matas-Diaz, "Voltage control of four-leg VSC for power system applications with nonlinear and unbalanced loads," *IEEE Trans. Energy Conv.*, vol. 35, no. 2, pp. 640–650, 2020.
- [18] K. D. Pippi, G. C. Kryonidis, A. I. Nousedilis and T. A. Papadopoulos, "A unified control strategy for voltage regulation and congestion management in active distribution networks," *Electr. Power Syst. Res.*, vol. 212, p. 108648, 2022.
- [19] A. M. Gross, K. N. Malamaki, M. Barragán-Villarejo, G. Kryonidis, F. J. Matas-Díaz, S. I. Gkavanoudis, J. M. Mauricio, J. M. Maza-Ortega and C. S. Demoulias, "Energy management in converter-interfaced renewable energy sources through ultracapacitors for provision of ancillary services," *Sustain. Energy, Grids and Networks*, vol. 32, p. 100911, 2022.
- [20] I. Vechiu, O. Curea and H. Camblong, "Transient operation of a four-leg inverter for autonomous applications with unbalanced load," *IEEE Trans. Power Electron.*, vol. 25, no. 2, pp. 399–407, 2010.
- [21] C. Demoulias, K. N. Malamaki, S. Gkavanoudis, J. M. Mauricio, G. Kryonidis, K. Oureilidis, E. Kontis and J. L. Martinez Ramos, "Ancillary services offered by distributed renewable energy sources at the distribution grid level: An attempt at proper definition and quantification," *Applied Sciences*, vol. 10, no. 20, 2020.
- [22] Documentation Simulink, "Simulation and model-based design," *MathWorks*, 2020. [Online]. Available: <https://www.mathworks.com/products/simulink.html>